Fire Star : a decision support system for fuel management and fire hazard reduction in mediterranean wildland - urban interfaces. Fire Star behaviour model of wildland fire. Experimental values of basic parameters

José Mendes Lopes, Claude Moro, J-Charles Valette, Joao Ventura

FIRE STAR

EVG1-CT-2001-00041

D5-01

http://www.eufirestar.org

FIRE STAR:

a decision support system for fuel management and fire hazard reduction in Mediterranean wildland - urban interfaces

Deliverable D5-01

Fire Star Behaviour Model of Wildland Fire

Experimental Values of Basic Parameters

José MENDES LOPES, Claude MORO,

Jean-Charles VALETTE, João VENTURA,

CONTENT LIST

SUMMARY

The main objectives of the work described in this document are:
- to get information on the flow inside the fuel complex for providing input information to the fire modellers,
- to determine the thermal degradation rate of different fuel families.

There are also the main objectives of WP5T1 task.

In section 2, the authors from IST-DEM describe the device they have elaborated for determining the heat transfer coefficients of the different types of wildland fuel beds according to porosity observed or/and measured outside.

They adapt to the device pressures taps along the duct for determining pressure drop per unit of length instead of drag coefficient, which need assumptions about the distribution of the needles.

In sections 3 and 4, INRA's authors describe the device they are using and the procedure they are following for determining the degradation rate of the different families of wildland fuel particles (leaves, very fine, fine and medium twigs).

The general trends are identical for all the "fine" fuels; coarser particles present a lower degradation rate.

GLOSSARY

porosity of the wildland fuel bed the ratio of the volume of the empty space inside the work module to the total volume of this work module

pressure drop per unit length the ratio of the difference of pressure measured at pressure taps to their distance along the duct; it will be substituted to the drag coefficient in the behaviour model of wildland fire

thermal degradation the decrease of the dimensionless ratio Mt-to-Mi (mass of the sample at the temperature T to the mass of the sample at ambient temperature)

thermal degradation rate this decrease per unit of increasing temperature

LIST OF ASSOCIATED DOCUMENTS

None

1 OBJECTIVES

The main objectives of the work described in this document are:

- to get information on the flow inside the fuel complex for providing input information to the fire modellers,
- to determine the thermal degradation rate of different fuel families.

1.1 FLOW INSIDE THE FUEL COMPLEX

Two important parameters, which are needed to model the flow inside the fuel matrix, are the heat transfer coefficient and the drag coefficient.

The fuel is placed inside a specially designed and built test section, connected to a fan through a heating module.

The controlling parameters are:

- Air flow velocity (used values between 1 ms^{-1} and 5 ms^{-1})
- Air temperature (between 293 K and 337 K)
- Fuel bed porosity (varied between 0.92 and 0.94)

The measured properties are:

- Pressure at several points along the working section, in order to get pressure drop values per unit length. Although we have obtained drag coefficients for the initial experiments in this rig, pressure drop per unit length is easier to obtain and does not need assumptions about the needles distribution. This change has been proposed to the modellers and accepted by them.
- Temperature at several points along the working section, from which heat transfer coefficients can be obtained.

There are some properties of the fuel and of the fuel matrix that are provided by our partners in the project (such as fuel density, calorific heat capacity, surface-to-volume ratio, …)

1.2 THERMAL DEGRADATION RATE

The first objective of this operation is to establish the relation between the rate of thermal degradation versus temperature of each type of fuel particle.

The second objective is to compare the results o different fuel particles.

These information may improve the predict ability of the behaviour model of wildland fire in better describing the combustion phase.

2 PHYSICAL PROPERTIES OF THE FUEL COMPLEX

2.1 INTRODUCTION

Surface fire is very important in forest fire ignition and propagation.

The surface fuel bed is a porous medium where a flow of air and gaseous combustion products is established during fire propagation.

The temperatures of the gas and of the fuel bed are not the same, especially in the vicinity of the flame: therefore, heat transfer occurs.

This exchange of energy plays an important role in the heating (or cooling) of the fuel bed, in the decrease of fuel moisture content and in its pyrolysis.

To model this gaseous flow, values of the coefficient of convection heat transfer and of the drag coefficient of the particles that form the fuel bed matrix are needed.

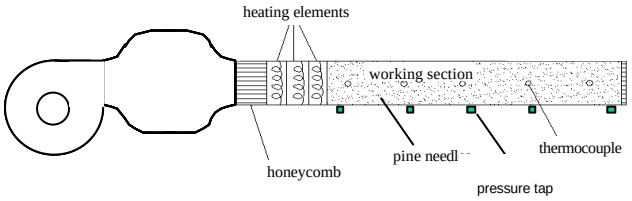

Figure 2-1: Experimental rig (schematic – not to scale)

Figure 2-2: Work module filled with needles
a) with the top cover removed; b) ready to work

2.2 THE EXPERIMENTAL DEVICE

The equipment used to obtain this data will be described in the present section.

The experimental rig used in this work is composed by three modules (Figure 2-1):

The fan module, comprising an electric motor, a fan, a plenum chamber and a contraction bringing the cross section down to 240 mm X 160 mm (width X height).

This equipment, already existing in our lab, was connected to the two following modules, which have been designed and built for the present set of experiments.

The heating module, consisting of a short duct 330 mm long, directly bolted to the contraction exit, contains a set of 15 electrical resistors with an overall power of 5 kW.

The electrical power can be varied by means of an AVAC rheostat.

The work module is a duct with the same cross section (240 mm X 160 mm) and 1.00 m long, made from 1.5-mm thick steel plate.

The top face is removable to allow the duct to be loaded/unloaded with needles.

This top cover is clamped to the main body of the work module.

To avoid the needles to be moved by the air flow, the entrance and exit sections of this module is closed with wire mesh.

The walls of the work module are thermally insulated with a rock wool layer 2-cm thick.

Figure 2-2 shows the work module:
- a) with the top cover removed and
- b) ready to work.

The work module is instrumented with five pressure taps and six thermocouples.

2.2.1 Preparation of the fuel matrix

In the laboratory, the needles are kept in cardboard boxes.

Before being loaded into the working section, they are left in the open air.

It can be safely assumed that the needles are in equilibrium with the ambient air.

The needles are weighted to determine the amount necessary to obtain the required matrix porosity.

The top of the working section is then removed and the needles are dropped by gravity.

The needles are uniformly compressed until they all fit inside the working section.

2.2.2 Main parameters

The main parameters used in the present work are:

- Porosity of the bed, defined as the empty volume inside the work module as a percentage of the total inner volume of this module.

$$\varepsilon = \frac{V_{empty}}{V_{total}} = \frac{V_{total} - V_{needles}}{V_{total}}$$

- Air flow velocity through the needles matrix: due to the difficulty of measuring inside the bed, flow velocity was measured at the exit of the work module (U_{aver}) and the velocity inside ($U_{needles}$) was deduced by using continuity equation.
- Air flow temperature.

2.2.3 Velocity measurements

The exit section of the work module is divided in six zones, measurements of velocity are taken in each zone with the thermo-anemometer.

The mean of these six measurements is taken as a representative value (U_{aver}).

The inlet valve to the fan enclosure controls airflow.

Applying continuity equation between the exit section and a generic cross section inside the work module

$$\rho A_{exit} U_{aver} = \rho \left(A_{exit} - A_{needles}\right) U_{needles}$$

where

- $A_{needles}$ is the projected area of the needles in the cross section plane and
- $U_{needles}$ is the velocity inside the fuel bed.

For these values of flow velocity, airflow is incompressible, density is constant and after some algebra we get

$$U_{needles} = \frac{U_{aver}}{\varepsilon}$$

2.2.4 Thermocouples and instrumentation

The above mentioned six thermocouples are located along the axis of the tunnel.

- the first of them is positioned at the beginning of the working section,
- the last is located 25 mm from the exit, and
- the four remaining ones are equally spaced between those two.

The thermocouples are K type.

The wire has a diameter of 0.25 mm with a spherical joint of 0.70 mm.

These dimensions present the best compromise between mechanical robustness (needed to withstand the loading and removing of the needles) and an acceptable time response.

The wires of the six thermocouples are connected to a Campbell Scientific data logger, model CR10.

This is a programmable unit with a memory capacity of approximately 29 990 values and six connections for voltage measurements in differential mode.

The sampling rate is one measurement per second per thermocouple (i.e. eight measurements per second overall).

The velocity of the air at the exit of the tunnel is measured with a Testo 425 hot wire thermo-anemometer.

The data from the data logger is downloaded into an Excel file.

All the data processing is carried out using the Excel software.

2.3 HEAT TRANSFER COEFFICIENTS

2.3.1 Analysis of the problem

Consider a small volume inside the matrix containing solid and gaseous phases.

An energy balance inside that volume indicates that the amount of thermal energy transferred from the air (gaseous phase) to the needles (solid phase) is equal to the amount of energy that raises the temperature of the needles:

$$A_n\, h\left(T_a - T_n\right) = \rho_n V_n c_{pn}\left(\frac{dT}{dt}\right)_n$$

where

- A_n is the area and V_n is the volume of the needles,
- ρ_n and c_{pn} are the density and the specific heat capacity of the needles.

The surface to volume ratio of the needles SVR_n is known, as well as ρ_n and c_{pn}.

The temperature of the air T_a can be measured and, hence, the derivative will be known.

The temperature of the needles T_n is very difficult to measure, as well as the derivative $(dT/dt)_n$.

Therefore, it is assumed that $(dT/dt)_n$ is equal to $(dT/dt)_a$.

This assumption can be justified because the Biot number of the needles is very low.

The convective heat transfer coefficient h is usually obtained from a Nusselt number.

In the literature, *Nu* is expressed as a relation between other non-dimensional numbers and some normalised (non-dimensional) characteristics of the geometry and properties of the flow.

Here the results are presented in this standard way.

Special care is needed to obtain the time constant of each thermocouple for each velocity situation.

2.3.2 Results

The value of h is obtained from the energy balance mentioned, and the Nusselt number is then computed.

For *Pinus pinaster* the following correlation between *Nu* and *Re* was obtained for a porosity of 95% and for *Re* in the range of 50 to 400 taking the linear dimension as $4/SVR$ of the needles:

$$\mathrm{Nu} = 0.1417\ \mathrm{Re}^{0.6053}$$

Values of h obtained from this correlation are around 30% to 40% of the values found in the literature for packed beds.

This difference was expected due to the much higher capacity of the packed beds (Figure 2-3).

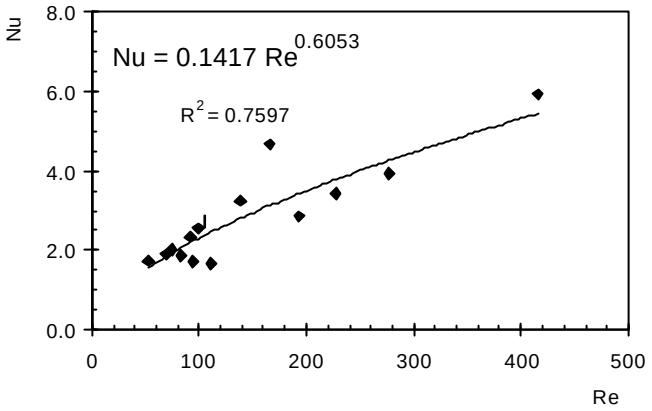

Figure 2-3: Computed values of Nu as a function of Re (T_{amb} = 22ºC, T_{hot} = 60ºC, matrix porosity = 0.95, *Pinus pinaster* needles)

2.4 PRESSURE DROP

2.4.1 Pressure measurements

The work module was provided with five static pressure taps, connected to a Furnace Control FCO 12 micromanometer, to check linearity in pressure drop along the duct.

After this check, only pressure drop values between the two extreme pressure taps have been used.

Figure 2-4 shows ΔP along the tunnel as a function of internal velocity for different porosity values.

The adjusted curves are second order polynomials.

2.4.2 Temperature measurements

Some experiments were carried out with airflow temperature in the range 293 to 337 K.

In steady state, the temperature at the exit section was measured with a digital thermometer, and five experiments, separated by 10 K, were performed for each value of porosity.

The set of experiments for each porosity value was carried out with the air inlet valve at a fixed position, corresponding to the middle velocity for the experiments at constant temperature.

It was found that the influence of the temperature on the pressure drop is relatively small for the range of temperatures used.

2.4.3 Calculations

Using the standard definition, the drag coefficient for an average sized needle is

$$C_D = \frac{F_{needle}}{\frac{1}{2}\rho U_{needles}^2 A_P}$$

where

- F_{needle} is the force acting on a single needle,
- ρ is the air density,
- $U_{needles}$ is the flow velocity inside the bed, and
- A_P is the average projected area, which the needles present to the flow.

Using average dimensions for the needles (considered as cylinders) and making a simplifying assumption about the needles distribution in the matrix, an expression was obtained for the average drag coefficient of a pine needle in a matrix as a function of flow velocity inside the needles bed and the flow temperature.

$$C_D = \left(-0.1546 \times U_{needles} + 1.3971\right)\left[0.5087 \times \left(\frac{T}{293}\right) + 0.4913\right]$$

This expression is valid for the range of parameters covered by the set of experiments, namely

- Porosity $0.92 \le \varepsilon \le 0.94$
- Flow velocity $1.15 \le U_{needles}\,[m/s] \le 2.48$
- Flow temperature $293 \le T\,[K] \le 337$

However, it has been agreed that in future work in this area, results should be expressed as pressure drop per unit length instead of a drag coefficient, as in the first case no assumptions are needed.

It has also been decided not to include the influence of temperature, because in the temperature range of interest, that influence is quite negligible.

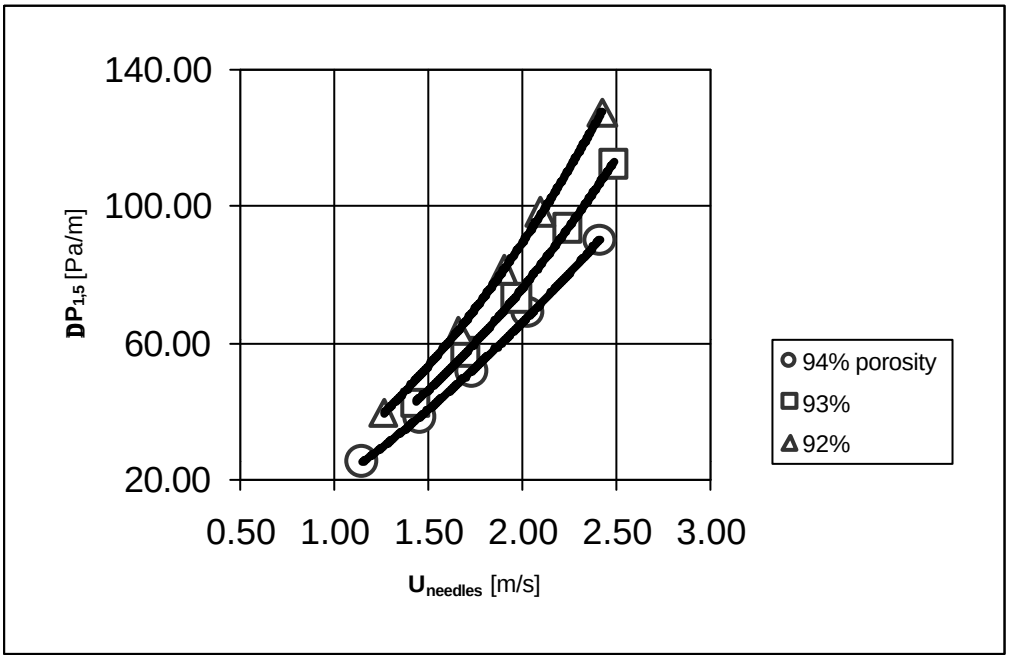

Figure 2-4: Pressure drop along the work module,
as a function of airflow velocity, for three different values of porosity.

3 THERMAL DEGRADATION RATE: METHOD

3.1 PROCEDURE

It has been described in D6-01 deliverable

3.1.1 Principle

We expose each series of five sample to increasing heat from the ambient to one of the thirteen following levels: from 373 to 973 K, step 50.

We plot the five dimensionless Mt-to-Mi ratios against their temperature level and analyse the shape of the obtained curve.

3.1.2 Preparation of the samples

Before carrying out this measurement, we put the samples in the drying oven (24 hours, 60°C) for working with oven-dried material.

3.1.3 The measurement itself

We constitute 5-g samples of oven-dried material and put them in each series of five cold molybdenum containers.

Then, we put the filled containers in the muffle furnace at ambient temperature and close the front door.

We fix the requested internal temperature and put on the furnace; the temperature increases at 100°K per hour, 1.7 K min^{-1}.

As soon as the internal temperature reaches the studied level (see table here below), we follow the same procedure as for determining ash content:

- to take the hot containers out of the furnace,
- to cover each of the containers with an aluminium sheet for avoiding to loose any particle,
- to place them in the vacuum chamber,
- to wait until the temperature of the containers returns to ambient.

The duration of this last phase depends on the level of the requested temperature.

We determine the “current” mass of each sample on cold material.

We carry out the same operations for each of the thirteen temperature levels.

Effective Temperature in °C	Displayed Temperature at C19 controller in °C
100	105
150	162
200	218
250	273
300	326
350	381
400	436
450	489
500	541
550	593
600	640
650	675
700	700

3.2 DEVICES

Figure 3-1: Electronic balance

Figure 3-2: The furnace and its electronic controller and the five containers

Figure 3-3: Vacuum chamber containing the five containers

4 THERMAL DEGRADATION RATE: RESULTS

4.1 AVERAGE VALUES

	Pinus eldarica needles Avignon Vaucluse France	Pinus halepensis needles Avignon Vaucluse France	Pinus halepensis needles Avignon Vaucluse France collected in 1999 used in July 2002	Pinus pinaster needles Gargas Vaucluse France	Pinus pinaster needles Gargas Vaucluse France used in July 2000	Pinus pinaster needles Gargas Vaucluse France collected in 2002 used in April 2003	Pinus pinea needles Lambert Var France	Quercus coccifera leaves Beauchamps B-d-Rhône France 2001	Quercus coccifera twigs 0-2 Beauchamps B-d-Rhône France 2001	Quercus coccifera twigs 2-6 Beauchamps B-d-Rhône France 2001
T en K	Mt/Mi	Mt/Mi	Mt/Mi	Mt/Mi	Mt/Mi	Mt/Mi	Mt/Mi	Mt/Mi	Mt/Mi	Mt/Mi
373,15	96,91	97,36	-	97,09	96,91	-	96,61	97,07	97,32	98,36
423,15	92,00	91,11	89,69	93,46	92,06	-	92,28	89,38	90,69	92,35
473,15	70,81	71,17	72,59	75,64	73,00	73,82	70,44	70,10	68,75	68,33
523,15	51,05	53,16	54,77	51,43	49,95	51,24	51,63	48,80	50,49	47,30
573,15	40,17	42,72	43,82	40,61	40,63	41,08	37,64	34,48	43,66	37,05
623,15	27,13	31,73	33,97	29,27	29,71	31,27	26,70	16,89	32,01	24,41
673,15	19,43	21,66	23,87	18,98	24,09	22,91	21,30	10,31	20,60	23,29
723,15	14,74	12,84	16,63	10,49	16,49	-	14,61	3,73	15,88	15,12
773,15	9,25	6,51	-	5,71	8,43	-	7,52	3,71	13,53	11,19
823,15	4,74	4,13	-	2,74	4,69	-	4,53	3,37	7,29	8,82
873,15	3,97	3,71	-	2,09	2,54	-	4,19	2,90	4,56	5,46
923,15	3,33	3,07	-	2,07	2,38	-	4,05	2,74	3,70	3,70
973,15	3,48	3,44	-	2,23	2,30	-	3,93	2,83	3,64	3,49

	Quercus ilex leaves Trou du rat Lubéron Vaucluse France summer 2002	Quercus ilex twigs 0-2 Trou du rat Lubéron Vaucluse France summer 2002	Quercus ilex twigs 2-6 Trou du rat Lubéron Vaucluse France summer 2002	Quercus ilex twigs 6-25 Trou du rat Lubéron Vaucluse France summer 2002	Quercus suber bark (Saltus)	Pinus halepensis bark (Saltus)	Pinus halepensis écailles of the cone (Saltus)	Pinus halepensis twigs 2-6 (saltus) (Saltus)
T en K	Mt/Mi	Mt/Mi	Mt/Mi	Mt/Mi	Mt/Mi	Mt/Mi	Mt/Mi	Mt/Mi
373,15	96,65	-	97,01	97,74	98,66	97,19	97,69	97,60
423,15	90,44	-	91,17	92,82	96,26	90,02	93,34	90,57
473,15	67,29	69,58	67,57	68,08	84,15	69,26	68,91	63,00
523,15	48,87	52,23	48,98	45,45	73,08	57,67	49,48	40,31
573,15	38,67	43,70	41,52	38,17	50,13	46,11	40,60	32,19
623,15	25,32	35,16	32,44	33,11	35,16	35,38	28,67	24,77
673,15	21,02	-	25,85	26,84	24,55	28,15	19,57	18,61
723,15	14,25	-	21,47	21,42	14,71	22,11	12,67	9,01
773,15	4,36	-	16,61	16,59	8,26	11,94	4,69	7,89
823,15	4,23	-	12,00	14,94	5,16	10,13	1,80	5,65
873,15	3,63	-	9,21	12,30	1,56	4,17	0,48	2,90
923,15	2,89	-	7,20	10,34	1,33	3,22	0,53	2,59
973,15	2,92	-	6,33	6,00	1,63	2,90	0,54	2,39

4.2 GRAPHS

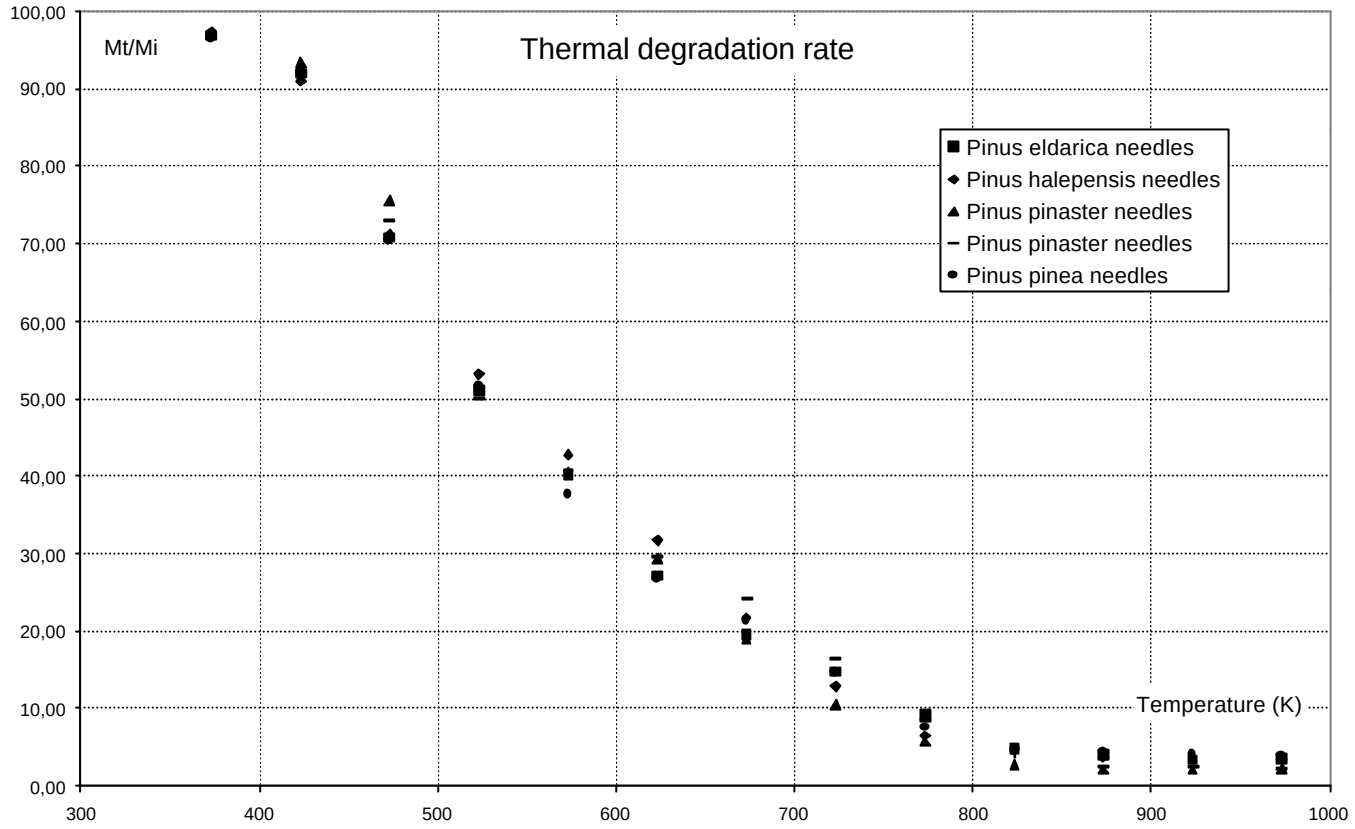

Figure 4-1: Thermal degradation rate for pine needles

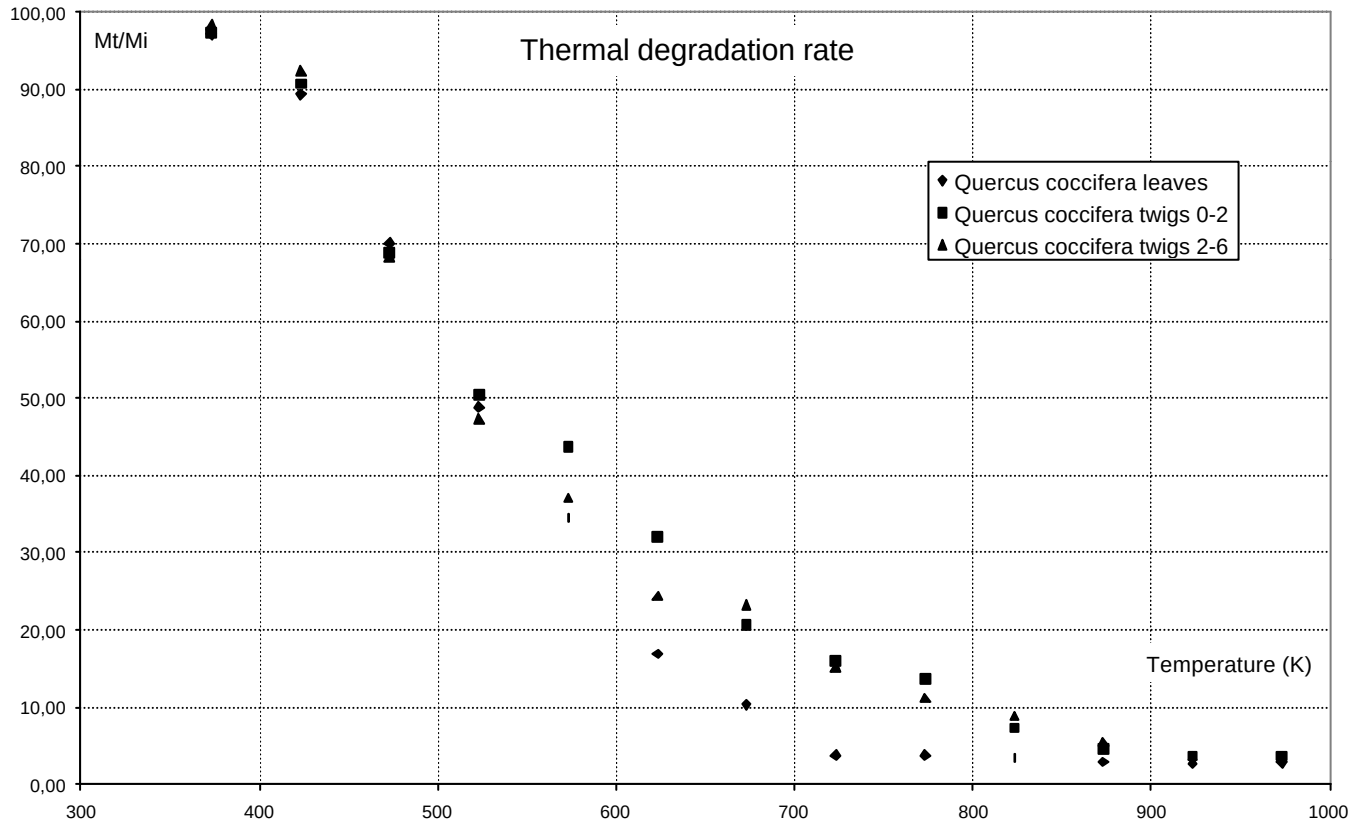

Figure 4-2: Thermal degradation rate of particles families of Quercus coccifera

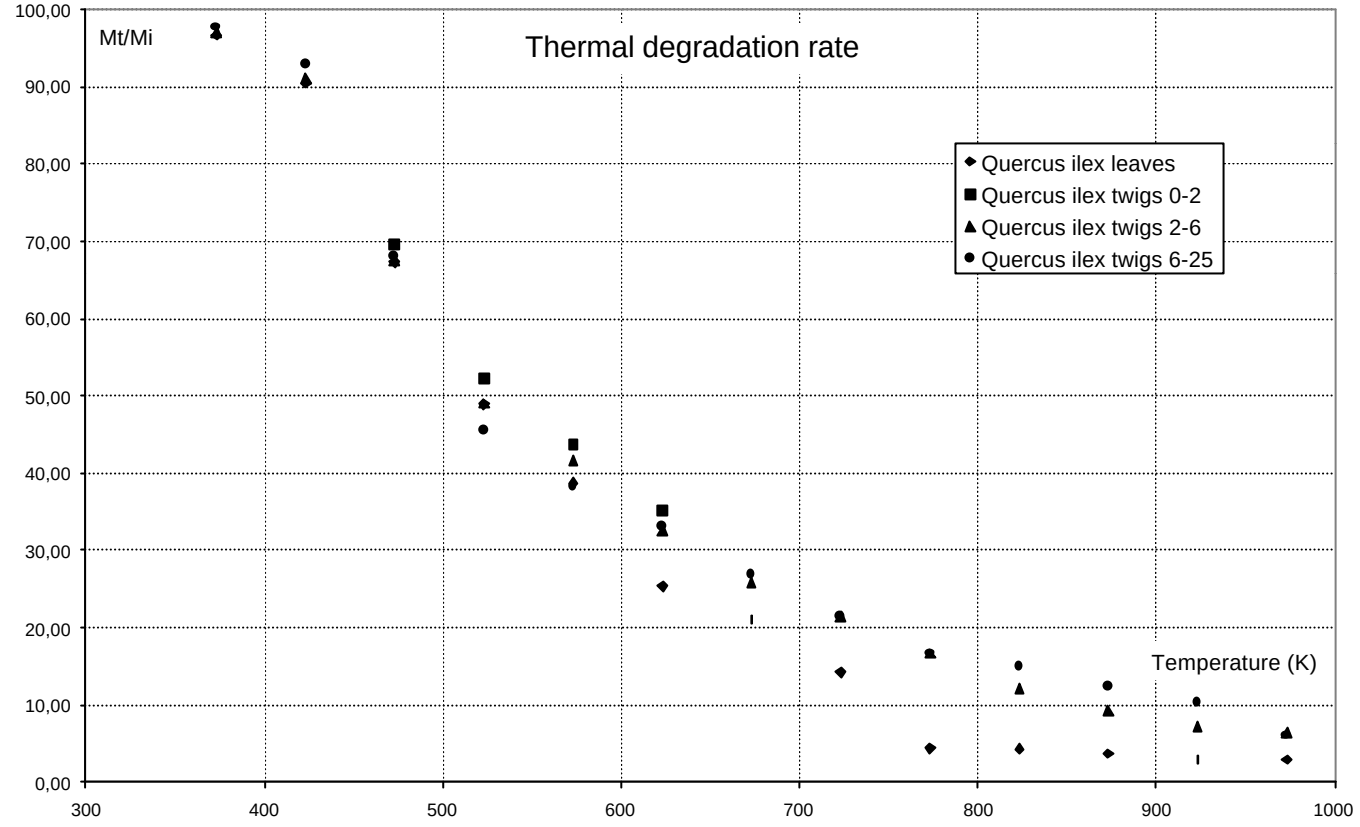

Figure 4-3: Thermal degradation rate of particles families of Quercus ilex

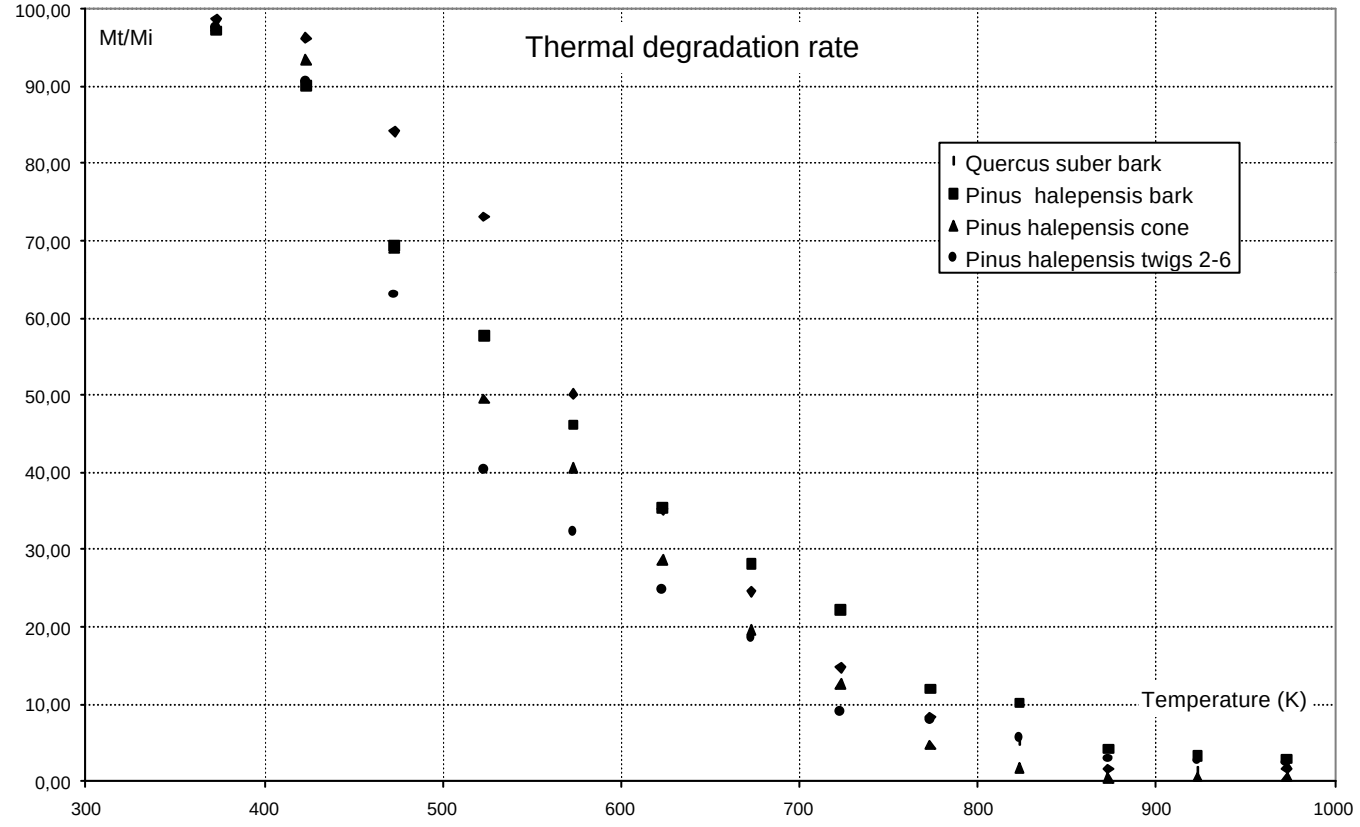

Figure 4-4: Thermal degradation rate of miscellaneous fuel particles families